NeuroImage **15,** 575–586 (2002)
doi:10.1006/nimg.2001.1013, available online at http://www.idealibrary.com on IDEAL®

Visually Evoked Gamma Responses in the Human Brain Are Enhanced during Voluntary Hyperventilation

Ole Jensen,* Riitta Hari,*,† and Kai Kaila‡

*Brain Research Unit, Low Temperature Laboratory, Helsinki University of Technology, FIN-02015 HUT, Helsinki, Finland; †Department of Clinical Neurophysiology, Helsinki University Central Hospital, Helsinki, Finland; and ‡Department of Biosciences, University of Helsinki, Helsinki, Finland

Received April 10, 2001

Hypocapnia induced by hyperventilation (HV) has powerful effects on neuronal excitability and synaptic transmission. We have studied the effect of hyperventilation on the phase-locked oscillatory components of the evoked responses in the human brain. We recorded visually evoked magnetoencephalographic responses before, during, and after voluntary hyperventilation to pattern-reversal checkerboard stimuli. Gamma-band (30–45 Hz) responses phase-locked to the stimuli were generated in the occipital visual cortex. A wavelet-based time-frequency analysis revealed that the gamma responses increased during HV whereas their frequency did not change significantly. A recent *in vitro* study in the rat hippocampus demonstrated that the stability of spontaneous gamma activity increases during hypocapnia as a result of enhanced GABAergic transmission. To test if a similar mechanism could account for our findings, we performed simulations on a network of 100 Hodgkin–Huxley neurons connected by inhibitory synapses. We found that enhanced $GABA_A$ transmission, paired with enhanced excitability, can explain the increase in evoked gamma activity without changing the frequency.

INTRODUCTION

Hyperventilation (HV) is known to lead to alterations in physiological and cognitive functions. For instance, cognitive performance was reduced in a Stroop-like task following a period of voluntary HV (Diest *et al.*, 2000). HV can provoke seizures in susceptible individuals and epileptiformic brain activity in the electroencephalogram (EEG) (Niedermeyer and Lopez da Silva, 1993). In EEG studies, visually evoked potentials in response to pattern reversals have been shown to remain unchanged during HV (Davies *et al.*, 1986; Gavriysky, 1991). In a recent magnetoencephalographic (MEG) study, voluntary HV reduced cortical auditory evoked fields, except for the 60-ms deflection which increased slightly (Huttunen *et al.*, 1999).

The HV-induced physiological changes are thought to be a consequence of increased neuronal excitability resulting from the hypocapnia-induced alkalosis (for reviews, see Wyke, 1963; Chesler and Kaila, 1992; Somjen and Tombaugh, 1998). Despite these findings, little is known about the physiological changes at the neuronal network level following HV.

In a recent *in vitro* study in the rat hippocampus the stability of spontaneous gamma activity (20–80 Hz) increases during hypocapnia as a result of enhanced GABAergic transmission (Stenkamp *et al.*, 2001). This finding is consistent with a large body of experimental and theoretical work on the generation of neocortical and hippocampal gamma oscillations in the rat (for reviews see Traub *et al.*, 1999; McBain and Fisahn, 2001). It has been established that the duration of the GABAergic inhibition determines the period of the gamma oscillations and that the GABAergic connections between the interneurons serve to synchronize neuronal spiking. We undertook the present study to find out whether a similar mechanism would be responsible for producing evoked gamma activity in the human visual cortex. We will demonstrate that visual stimulation evokes responses in the gamma band and that these responses are clearly modulated by HV.

To investigate possible neuronal mechanisms we implemented a network model, introduced by Wang and Buzsaki (1996) and based on coupled inhibitory neurons of the Hodgkin–Huxley type (Hodgkin and Huxley, 1952). This model was originally designed to account for spontaneous gamma oscillations in the rat hippocampus, but as we will show, it can also generate evoked gamma responses similar to those we observe in the visual cortex. By manipulating the efficacy of $GABA_A$ receptor-mediated inhibition and the neuronal excitability, we were able to explore plausible physiological mechanisms which could explain the experimental findings.

1053-8119/02 $35.00

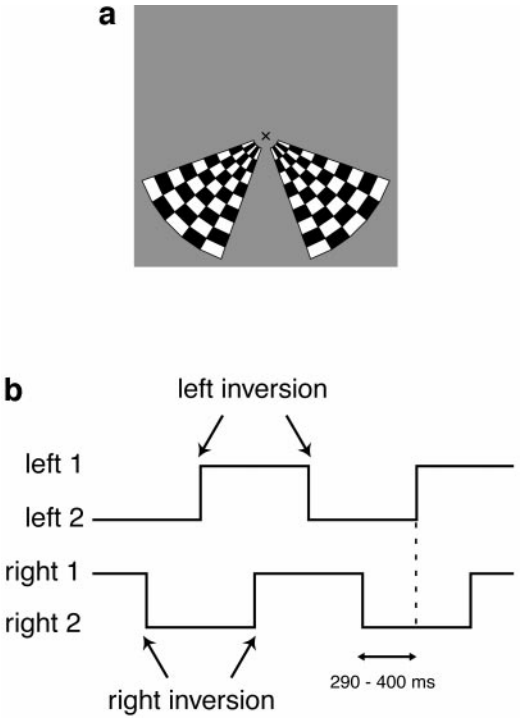

FIG. 1. (a) The pie-shaped checkerboard patterns applied as visual stimuli. (b) Every 290–400 ms, the black and white fields of the checkerboards were inverted, alternatingly, either in the LVF or RVF.

METHODS

Subjects. Magnetoencephalographic (MEG) signals were recorded from eight healthy subjects (ages 25–32, mean 28.9 years, 5 males, 7 right-handed) who had no history of neurological disorders. Informed consent was obtained from each subject after full explanation of the study.

Stimuli. Pie-shaped sectors of black and white checkerboards, as shown in Fig. 1a, were used as visual stimuli. The stimuli extended from eccentricities of 4° to 14°. The luminances of the black, white, and gray areas were 1, 60, and 30 cd/cm^2, respectively. The stimuli were produced by a computer outside the room and projected onto a semitransparent projection screen placed 100 cm in front of the subject. The checkerboards were continuously shown, but every 290–400 ms the black and white checks were inverted, alternatingly in the left and the right visual field (LVF and RVF), as illustrated in Fig. 1b. Pattern-reversals in the lower left and right visual fields elicited strong magnetic brain responses in a previous study (Portin *et al.*, 1999).

Task. The subjects were asked to focus on a cross at the center of the screen. The cross changed randomly from black to white in about 1 of 20 inversions. After each recording session, the subjects were asked to report the number of times the cross had changed.

Hyperventilation. Prior to the recordings, but never on the same day, the subjects had practiced voluntary HV for a 3-min period by breathing deeply at a constant rate (Bostem, 1976). Each subject participated in two sessions. During the first 6-min control session, the checkerboards were inverted 500 times in each visual field. Following a break of about 5 min, the subjects were asked to hyperventilate during a 3-min period, while the visual stimuli were presented continuously (≈250 reversals per visual field). This was followed by a 3-min period of normal breathing while the visual stimulation continued (≈250 reversals per visual field).

Data acquisition. MEG signals were recorded with a helmet-shaped 306-channel detector array (Vectorview, Neuromag Ltd, Helsinki, Finland). This system has 102 sensor elements distributed over the scalp, each with two planar gradiometers and 1 magnetometer and thereby 3 SQUIDs (superconducting quantum interference devices). For a review on the MEG technique, see Hämäläinen *et al.* (1993). To measure the location of the head with respect to the sensors, four coils were placed on the scalp. The relative positions of the coils with respect to anatomical landmarks on the head were determined with a 3-D digitizer. After the subjects were seated under the MEG helmet, the positions of the coils were determined by measuring the magnetic signals produced by the coils when a current was passed through them. Magnetic resonance images (MRIs) were obtained from three subjects with a 1.5 T Siemens Magnetom scanner and were aligned to the MEG coordinate system according to anatomical landmarks.

Eye-blink artifacts were monitored by recording the vertical electro-oculogram (EOG). The EOG and stimulus markers were stored together with all MEG signals for off-line analysis. The signals were bandpass filtered from 0.1 to 100 Hz and digitized at 300 Hz. Interference from external magnetic fields was suppressed using principal component analysis by which components of interfering noise sources were calculated for empty room recordings. These components were applied to create linear projections to reduce the contribution from external noise sources (Parkkonen *et al.*, 1999).

Data analysis. The first part of the data analysis concentrated on source modeling of the visually evoked fields (VEFs) filtered both in the wide-band and a narrow gamma-band (30–45 Hz). Since we assumed that the location of the sources producing the VEFs did not change during HV, signals from the control and HV conditions were averaged before source localization. Epochs containing EOG signals in excess of ±75 μV were ignored from the analysis. VEFs were obtained by averaging the signals time-locked to the pattern-rever-

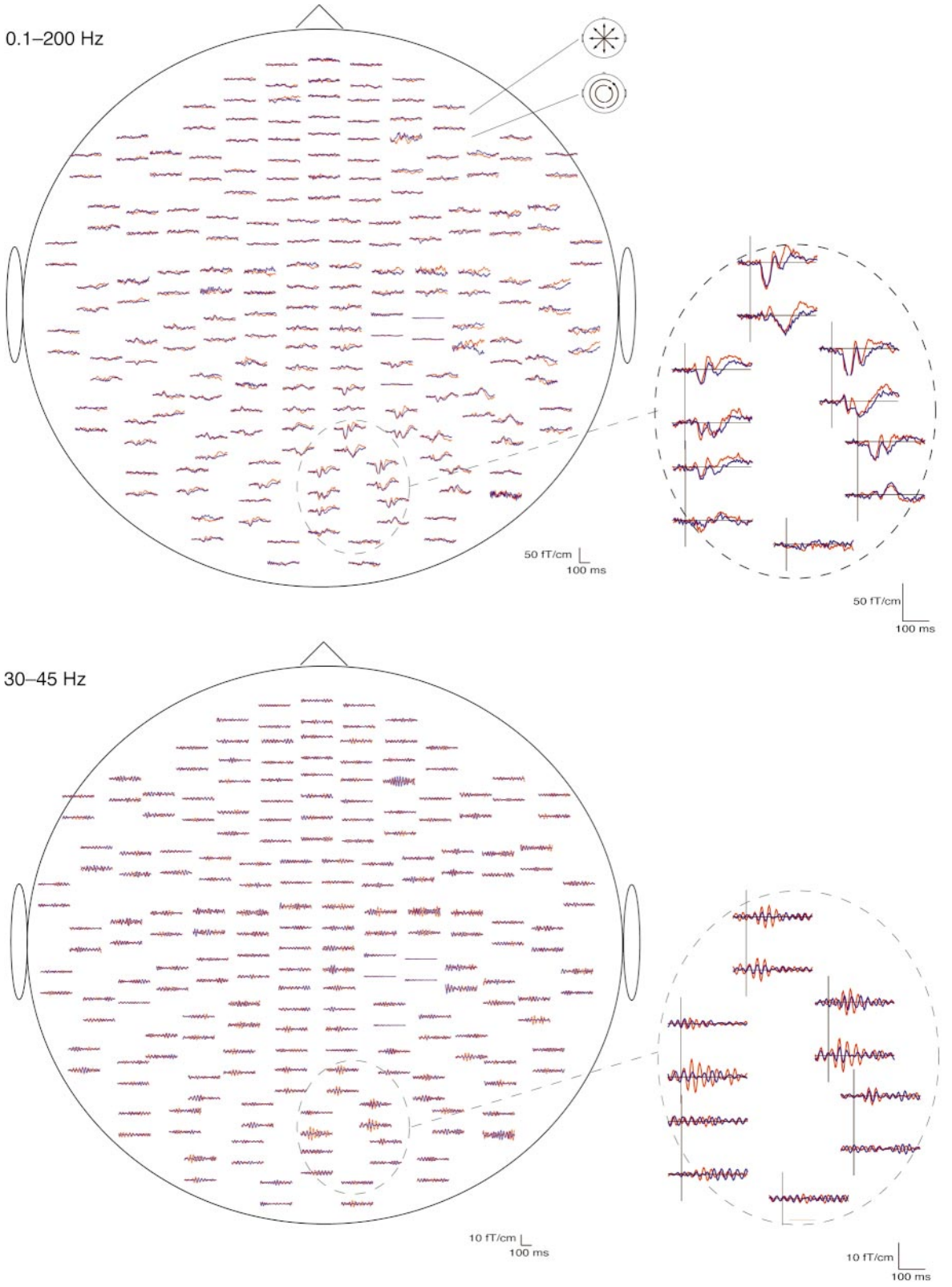

FIG. 2. VEFs from Subject 1 to LVF pattern-reversals presented during the control (blue) and HV condition (red). The responses were filtered through 0.1–200 Hz to display the "wide-band" responses (top) and through 30–45 Hz to display the "gamma" responses (bottom).

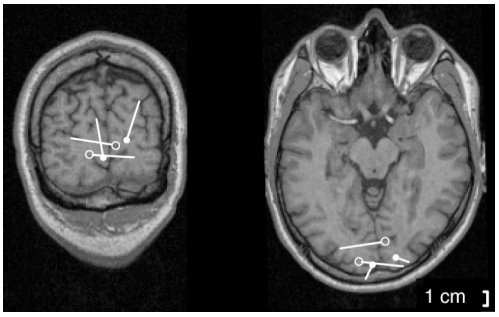

FIG. 3. Equivalent current dipoles (ECDs) modeling the wide-band (filled symbols) and gamma-band VEFs (open symbols) for Subject 1. Coronal (left) and horizontal (right) cuts are shown. The dipoles in right hemisphere are for the VEFs in response to checkerboard inversion in the LVF and vice versa.

sals separately for the LVF and RVF stimuli. The amplitudes were measured with respect to a 50-ms baseline prior to the pattern-reversal. Sources of the averaged VEFs were modeled as equivalent current dipoles (ECDs) (Hämäläinen *et al.*, 1993), whose three-dimensional locations, orientations, and strengths were found in a least-squares search using signals from 60–80 sensors over the maximum response area. A 1- or 2-dipole model was applied to explain the wide- and gamma-band VEFs. A goodness-of-fit value (g) was calculated to indicate how well the model accounted for the measured field variance.

The ECDs were then introduced into a time-varying 1- or 2-dipole model, where the dipole strengths were allowed to vary as a function of time. This model was used to explain the measured signals in all 306 sensors prior to averaging. In other words, the time-varying dipole model served as a "spatial filter" with which we extracted altogether ~500 single trial source waveforms (i.e., time courses of the identified current dipoles) time-locked to the pattern reversals.

Time-frequency representations (TFRs) of the single trials were calculated using wavelet techniques (Kronland-Martinet *et al.*, 1987; Sinkkonen *et al.*, 1995) that for instance have been applied to characterize visually induced oscillatory EEG activity (Tallon-Baudry and Bertrand, 1999).

The TFR of the power $P(t, f_0)$ for a given signal at time (t) and frequency (f_0) is given by the squared norm of the convolution of a Morlet wavelet, $w(t, f_0) = A\exp(-t^2 2\sigma_t^2)\exp(2i\pi f_0 t)$ to the signal $s(t)$:

$$P(t, f_0) = |w(t, f_0) \times s(t)|^2, \tag{1}$$

where $\sigma_f = 1/(2\pi\sigma_t)$ and $A = 1/(\sigma_t\sqrt{2\pi})$. We chose the "width" of the wavelet ($m = f_0/\sigma_f$) to be 7. The TFRs were calculated for the individual trials time-locked to the pattern reversals and then averaged. The power calculated in the interval −100 to 0 ms prior to the pattern reversal was subtracted from the TFRs. This procedure allows to detect induced oscillatory activity that is not necessarily phase-locked to the pattern reversals.

The phase-locking factor (PLF) was applied to determine whether the signals at a given frequency (f_0) and time (t) are phase-locked to the pattern reversals. The normalized complex representation of the time-locked signal, convoluted to the wavelet, was calculated and then averaged over multiple trials:

$$\Phi(t, f_0) = \frac{1}{N}\sum_{i=1}^{N}\frac{w(t, f_0) \times s_i(t, f_0)}{|w(t, f_0) \times s_i(t, f_0)|}. \tag{2}$$

The modulus (absolute value) of this measure varies between 0 and 1 and defines the degree of phase-locking. Statistical significance of the PLF was established using a bootstrapping method. For 500 traces ($N = 500$), a PLF above 0.10 is statistically significant at $P = 0.01$. When comparing two PLFs (each calculated from about 500 traces), differences above 0.09 are significant at $P = 0.01$.

The network model. To test theoretical ideas on neuronal synchronization underlying the phase-locked gamma responses, we implemented a network model introduced by Wang and Buzsaki (1996). Originally this model was constructed to explain ongoing spontaneous gamma activity generated by networks of coupled inhibitory neurons, whereas we applied it to investigate evoked gamma responses. In the simulations of Wang and Buzsaki (1996), a tonic depolarizing cur-

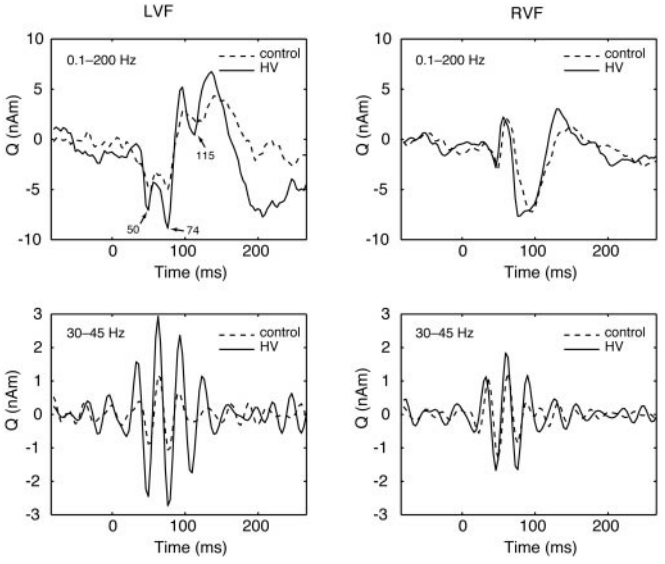

FIG. 4. The averaged strength of the time-varying dipoles modeling the gamma-band VEFs in Subject 1. The top panels show the wide-band VEF for the control and HV condition. The lower panels show the corresponding gamma-band VEFs.

TABLE 1

Source Location in Talairach Coordinates for the Wide-Band (0.1–200 Hz) and Gamma-Band (30–45 Hz) VEFs at 60–80 ms in Three Subjects

		LVF			RVF		
Subject	Band (Hz)	x (mm)	y (mm)	z (mm)	x (mm)	y (mm)	z (mm)
1	0.1–200	10	−86	10	−6	−93	−2
	30–45	10	−80	2	−2	−86	−10
2	0.1–200	1	−81	2	−6	−93	−4
	30–45				−16	−87	−3
7	0.1–200	−1	−95	−3	−20	−91	13
	30–45	−1	−91	−5	−14	−94	19

Note. All the coordinates agree with locations in the the V1/V2 cortex (Hasnain *et al.*, 1998).

rent was applied to every cell of the network, whereas we applied a short depolarizing current pulse to simulate the evoked responses. The membrane potential (V^i) of neuron i is described by a single-compartment model

$$\frac{dV^i}{dt} = \frac{1}{C_m}(-I^i_{\mathrm{Na}} - I^i_K - I^i_L - I^i_{\mathrm{syn}} + I^i_{\mathrm{app}}), \qquad (3)$$

where C_m is the membrane capacitance, and I_{Na}, I_K, I_L, I_{syn}, and I_{app}, respectively, refer to the sodium, potassium, leakage, synaptic, and input currents. The expression for each current, except for I_{app}, takes the form

$$I_x = g_x\,(V - E_x), \qquad (4)$$

where g_x is the membrane conductance and E_x is the reversal potential for a given current (x). The voltage-dependent kinetics of the sodium (g_{Na}) and potassium (g_K) conductances are modeled by equations of the Hodgkin–Huxley type (Hodgkin and Huxley, 1952; for details see Wang and Buzsaki, 1995). A depolarizing current pulse, I^i_{app}, of 100 ms, was applied simultaneously to each neuron. The amplitudes of the current pulses to each neuron were distributed around the mean $I_{\mathrm{app},\mu}$ with a standard deviation I_σ. The different depolarizing currents drove the uncoupled neurons at different firing frequencies. Increases in excitability were simulated by increasing $I_{\mathrm{app},\mu}$. In the first set of simulations we investigated the firing characteristics and degree of synchrony of the uncoupled cells in response to the current pulses. Then the cells were coupled with inhibitory GABAergic synapses. The $\mathrm{GABA_A}$ receptor-mediated synaptic current to cell i from cell j is expressed as

$$I^i_{\mathrm{syn}} = \sum_{j=1}^{N} g_{\mathrm{GABA_A}} s^j (V - E_{\mathrm{GABA_A}}), \qquad (5)$$

where s^j is the gating variable for the presynaptic cell j. When cell j fires (exceeds a threshold), s^j increases within a few milliseconds and then decays exponentially with a time constant $\tau \approx 10$ ms. All-to-all connections were applied and changes in inhibitory transmission were modeled by adjusting $g_{\mathrm{GABA_A}}$.

In cortical networks, the signals measured by MEG are mainly produced by currents parallel to the apical dendrites of cortical pyramidal neurons (Hämäläinen *et al.*, 1993). Direct contributions from currents flowing in less aligned cells, such as the inhibitory interneurons, are considered negligible. Experimental *in vivo* recordings of gamma activity in the rat hippocampus have shown that pyramidal neurons typically fire when the GABAergic inhibition from the interneuronal network decays sufficiently (e.g., Penttonen *et al.*, 1998). For the sake of simplicity, we did not model pyramidal neurons explicitly, but we assigned a magnetic field (B) with the time course of the net excitatory postsynaptic currents (EPSCs) to each spike produced by the interneurons. The EPSCs were modeled by alpha-functions (Koch and Segev, 1998). The total magnetic field $B(t)$ is then

$$B(t) \propto \sum_{i=1}^{N} \frac{t}{\tau} \exp\left(-\frac{t - t_{\mathrm{spike,\,i}}}{\tau}\right), \qquad (6)$$

where t^i_{spike} defines the time when inhibitory cell i crosses the firing threshold. The total field calculated by this method was then subjected to a time-frequency analysis as described earlier in this section.

The network was numerically integrated by a fourth-order Runge–Kutta method with 0.1 ms time-steps (Press *et al.*, 1997). For further details on the model and for justifications of parameter values, see Wang and Buzsaki (1996). Figure captions list parameters that differed from those applied by Wang and Buzsaki (1996).

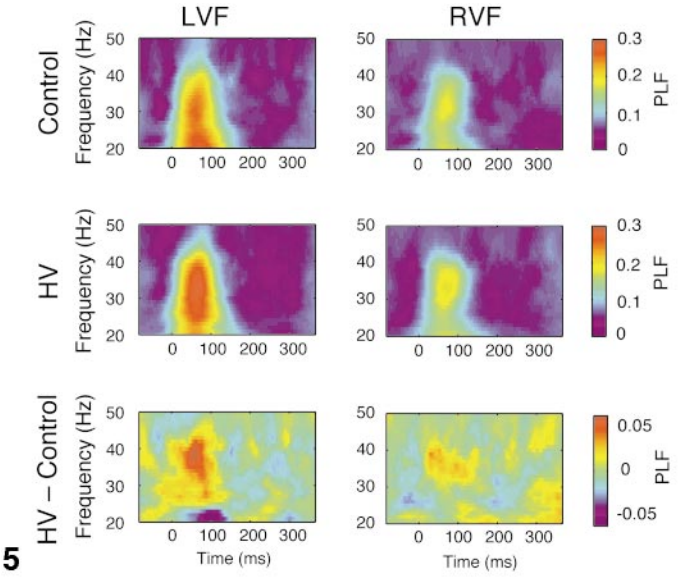

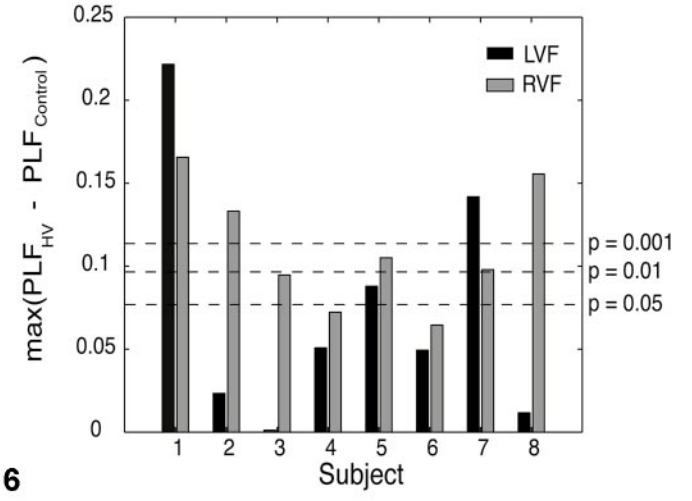

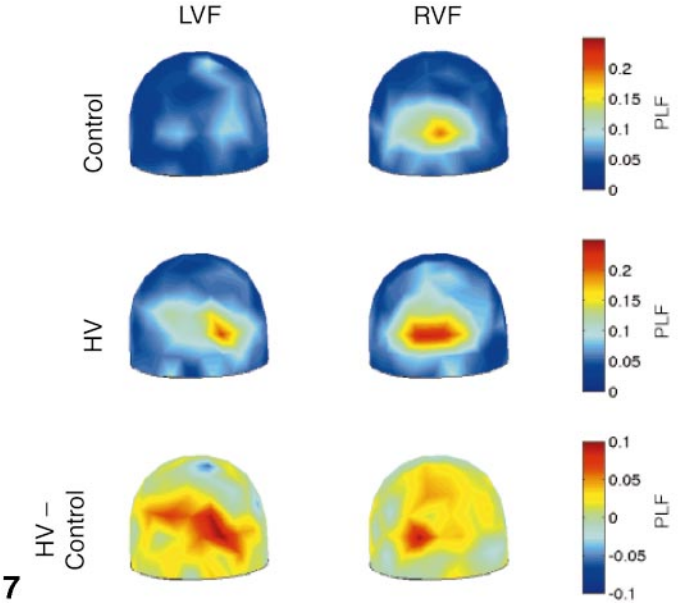

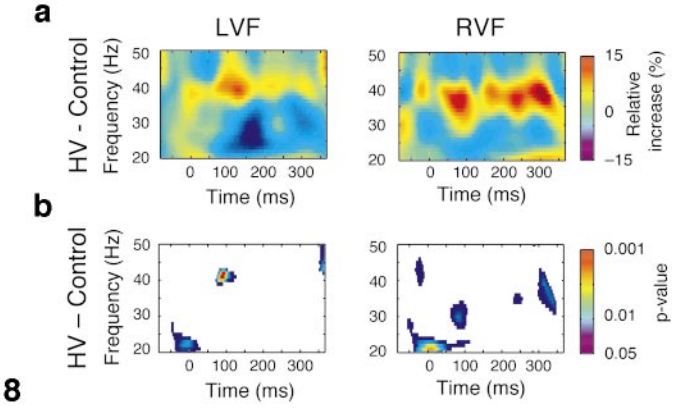

FIG. 5. The grand mean ($N = 8$ subjects) phase-locking factor (PLF) as a function of time. The PLF was calculated for the single trial source waveforms time-locked to the stimuli. The color code denotes the degree of phase locking. The left column refers to LVF and the right column to RVF stimuli. The PLF in the gamma band is higher during HV (middle row) than during the control condition (top row). The subtraction (HV minus control, bottom row) reveals that the increase in PLF is constrained to the 30–45 Hz band.

FIG. 6. The maximum increase in PLF with HV (HV minus control, $f = 30$–45 Hz, $t = 55$–75 ms). Black and gray bars correspond to LVF and RVF, respectively.

FIG. 7. Topography of the PLF in Subject 1. PLFs in the gamma band ($f = 35$–40 Hz, $t = 55$–75 ms) were calculated for the planar gradiometers and color-coded on a geometry corresponding to the MEG sensor array (viewed from the back). The areas over which the PLF increases includes areas of high PLF during HV and control.

FIG. 8. (a) Time-frequency representations (TFRs) of the relative increase in power with HV averaged over the 8 subject. The TFRs were calculated with respect to the time-varying dipoles as in Fig. 5. (b) A statistical measure for the power increase of the TFRs with HV.

RESULTS

Visually Evoked Fields and Source Modeling

Figure 2 shows VEFs of Subject 1 in response to LVF stimuli during the control and HV conditions. The traces are arranged topographically according to the relative position of the respective sensors. During both conditions, the wide-band VEFs peaked 60–80 ms after the stimuli. The strongest responses were observed over the right occipital cortex. The gamma-band VEFs

were obtained by bandpass filtering the VEFs from 30 to 45 Hz. Later, we will justify the choice of this frequency band by a time-frequency analysis. As shown in Fig. 2 (bottom; 30–45 Hz) the gamma-band VEFs were stronger during HV than control conditions.

Sources of the VEFs (control and HV condition averaged) were modeled at the peak latencies (60–80 ms) by single ECDs. Figure 3 (closed symbols) shows the locations and orientation of the ECDs for Subject 1. In 6 of 8 subjects, the goodness-of-fit exceeded 90% and in all subjects it exceeded 80%. In 7 subjects, the LVF stimuli consistently resulted in ECDs located in the right occipital cortex, and *vice versa*. Table 1 shows the Talairach coordinates (Talairach and Tournoux, 1988) of source locations for the three subjects for whom we had MRIs. The locations agree with area $V1/V2$ of the visual cortex (Hasnain *et al.*, 1998).

A 1-dipole model was sufficient to account for the gamma-band VEFs to either LVF or RVF stimuli in 5 of 8 subjects. Figure 3 (open symbols) shows the locations and orientation of the ECDs modeling the gamma responses in Subject 1. In the remaining three subjects, a 2-dipole model per hemisphere increased the goodness-of-fit substantially. Thirteen of the 16 dipole models accounted for gamma-band VEFs with a goodness-of-fit better than 80%. As shown in Table 1, the ECDs for the gamma-band VEFs were also located in area $V1/V2$. In Subject 2 it was not possible to model the gamma responses to RVF stimuli.

The ECDs for the wide-band and gamma-band VEFs were typically quite close to each other; the mean differences in location (gamma-band minus wide-band VEFs) were $x = -0.2 \pm 2.8$ mm, $y = 6.3 \pm 2.2$ mm, and $z = -8.7 \pm 3.6$ mm ($N = 8$) for LVF, and $x = 2.1 \pm 1.2$ mm, $y = 3.4 \pm 1.5$ mm, and $z = -1.6 \pm 6.7$ mm ($N = 7$) for RVF. The statistically significant difference ($P < 0.05$) in the y direction implies that the ECDs for the gamma responses were about 5 mm deeper than those for the wide-band VEFs.

As the next step, the strengths of the dipoles modeling the gamma-band VEFs were allowed to vary as a function of time to explain the signals in the 306 sensors. Figure 4 shows an example of the time courses of the $V1/V2$ dipoles for Subject 1. Even in wide-band VEFs, the gamma responses are apparent as deflections at 50, 74, and 115 ms, as indicated by the arrows. After bandpass filtering through 30–45 Hz it becomes evident that the gamma responses increased with HV (Fig. 4, bottom). In this subject, gamma responses increased more with HV to LVF than RVF stimuli.

The time courses of the evoked signals of the current dipoles were very similar to those characterized by Portin *et al.* (1998; 1999). In accordance with the EEG study by Davies *et al.* (1986), we were not able to detect consistent changes in onset or peak amplitudes of visual responses with HV.

Characterization of Gamma Responses

Bandpass filtering of evoked responses in a given frequency band is problematic since effects in other frequency bands are not visible, and since steep temporal gradients in the evoked fields can produce false signals in the filtered responses due to "filter ringing." To better characterize the gamma responses, we calculated the single source waveforms time-locked to the stimuli using the time-varying dipole models explained above. The single trial traces were then analyzed using the phase-locking factor (PLF). For subjects in whom a 2-dipole model was applied, the traces from the dipoles with the largest gamma responses were chosen for the analysis.

Figure 5 illustrates the grand-mean (eight subjects) time-frequency representations of the PLF for the control and HV conditions. The color code represents the degree of phase locking. Both during control and HV particularly strong PLF is seen below 40 Hz, 30–90 ms after the LVF pattern-reversals (left column). After RVF stimuli (right column), strong phase-locking is constrained to the 30–40 Hz band. HV increased the PLF as is evident from the difference plots (HV minus control, bottom panels). Interestingly, for LVF stimuli the increase was constrained to the 30–45 Hz band even though the PLF was relatively strong at 20–40 Hz. For Subject 6, the PLF differed from the grand average: during the control condition gamma responses were observed at 40 Hz, but during HV the response shifted to 50 Hz. The frequencies and times of the PLF peaks did not differ statistically significantly between control and HV conditions (control, left: 35.7 ± 1.6 Hz and 75 ± 7 ms, right: 37.9 ± 2.5 Hz and 78 ± 9.0 ms. HV, left: 37.0 ± 1.5 Hz and 65 ± 7.7 s, right: 37.1 ± 6.6 Hz and 67 ± 6.6 ms; differences, HV minus control, left: 1.3 ± 0.7 Hz and -10.4 ± 8.0 ms, right: -0.8 ± 1.7 Hz and -10.4 ± 11.9 ms).

To test the statistical significance of the gamma response changes with HV, we searched the maximum value from the PLF difference plots (HV minus control, corresponding to the bottom panel in Fig. 5) in the frequency interval from 30 to 45 Hz between and 55 and 75 ms. As shown in Fig. 6, the increase of gamma responses was significant ($P < 0.05$) in three subjects for both visual fields. In six subjects, the increase was statistically significant to stimuli in at least one visual field, and in two subjects no significant increase was observed.

To further characterize the spatial extent of the gamma responses and their increase, we calculated the PLF in all gradiometer coils for Subject 1 from 30 to 45 Hz between 55 and 75 ms. These values were then color-coded on a geometry corresponding to the locations of the sensors. Figure 7 shows that gamma responses were observed over the parieto-occipital re-

gions and that these areas did not appear to differ from areas in which the PLF increased during HV (lower panels).

To investigate whether the increases in PLF in the gamma band with hyperventilation were associated with increased signal amplitudes, we calculated the TFRs of the power changes in the source waveforms. The TFRs were calculated for the single-trial signals time-locked to the stimuli and then averaged. The relative changes in the TFRs were calculated and then averaged over the 8 subjects. Figure 8a shows a transient increase at 35–45 Hz 50–100 ms after LVF stimuli, for the RVF stimuli, the increase was sustained and occurred in a slightly lower frequency band (35–40 Hz). The changes in frequency bands with respect to LVF vs RVF stimuli were consistent with the findings using the PLF (see Fig. 5, lower panel). A *t* test was applied ($N = 8$) to each point in the TFRs to establish whether the relative increases in the TFRs were significant. The increase was significant at 38–42 Hz 50–100 ms after LVF stimuli (Fig. 8b). The significant increase below 25 Hz might be explained by a rebound of the ~20 Hz rebound which is suppressed by the stimuli. For RVF stimuli the increase with HV was significant in the 28–35 Hz band at 50–100 ms (Fig. 8a, right panel). Interestingly a significant increase was also observed around 300 ms. This is consistent with the sustained increase in the gamma band, and it suggests that not only phase-locked but also induced gamma band activity increases with HV. However, the validity of this finding deserves to be further explored, since RVF stimuli did not produce a similar effect.

The Model

A network model constructed of 100 Hodgkin–Huxley type model neurons (see Methods) was implemented to investigate the physiological mechanisms accounting for the increase in gamma responses during HV (Fig. 9a). When a short pulse of depolarizing current is provided to the model neurons, they spike. If the cells are uncoupled, they will fire with a frequency of about 60 Hz, as illustrated in Fig. 9b, which shows the voltage traces of 10 of the 100 neurons. The differences in firing frequency reflect variations of the input currents. Initially the cells fire synchronously, but the synchrony is lost within 100 ms. When the cells are coupled with $GABA_A$ synapses, the firing frequency slows down to about 40 Hz and the synchrony is maintained during the period of depolarization (Fig. 9c). In a recent hippocampal slice study, IPSCs increased in amplitude after hypocapnia, but their kinetics remained the same (Stenkamp *et al.*, 2001). In our model this effect is mimicked by an increase in $GABA_A$-mediated conductance. Thus, we explored the changes in gamma responses produced by the network model as a function of the inhibitory conductance (Fig. 10).

The top left panel of Fig. 10 shows that the gamma frequency of the evoked responses decreases from 52 to 42 Hz as the inhibitory conductance increases by a factor of 4. The lower left panel of Fig. 10 shows the equivalent changes in power. Initially, the evoked gamma response increases with GABAergic conductance, but with a further increase the gamma response eventually drops. From these simulations we conclude that an increase in GABAergic current can account for an increase in the amplitude of evoked gamma responses, but not without reducing the frequency. Hypocapnia is also known to produce an increase in neuronal excitability and excitatory transmission (Wyke, 1963; Chesler and Kaila, 1992; Lee *et al.*, 1996; Somjen and Tombaugh, 1998). Hence, we modeled an increase in excitability as an increase in input current.

Figure 10 (top panel, right) shows that the gamma frequency increases with input current. The evoked gamma response first increases and then decreases with the increase in excitatory drive. Thus, an increase in excitability can account for an enhanced evoked gamma response, but an increase in frequency is inevitable. We therefore propose that the decrease in frequency with enhanced GABAergic transmission during HV might be counterbalanced by an increase in excitability. The net result is an increase in gamma responses with negligible changes in the frequency.

Figure 11a shows the time-frequency representation of the power (see Methods) of the "control" condition where $g_{GABA_A} = 0.06$ mS/cm^2 and $I_{app,\mu} = 0.8$ μA/cm^2. In the state representing hypocapnia, modeled as an increase in GABAergic conductance ($g_{GABA_A} = 0.10$ mS/cm^2) and excitability ($I_{app,\mu} = 1.0$ μA/cm^2), the power of the evoked gamma responses is increased. The frequency does not change (Fig. 11b).

DISCUSSION

In six of eight of our subjects, visually evoked cortical responses constrained to the gamma band (30–45 Hz) increased during voluntary HV, with no systematic changes in the frequency or peak time of the response. The increase in the gamma responses was observed both when characterizing the responses using the phase-locking factor (PLF) and time-frequency representations (TFR). Thus the enhancement seems to be at least partly explained by an increase in the amplitude of the gamma responses. The phase-locked gamma responses were found to originate in the occipital *V*1/*V*2 cortex.

Which physiological mechanisms could explain the increase in evoked gamma responses during HV? HV is a consequence of excessive breathing that reduces the partial pressure of CO_2 (hypocapnia) leading to respi-

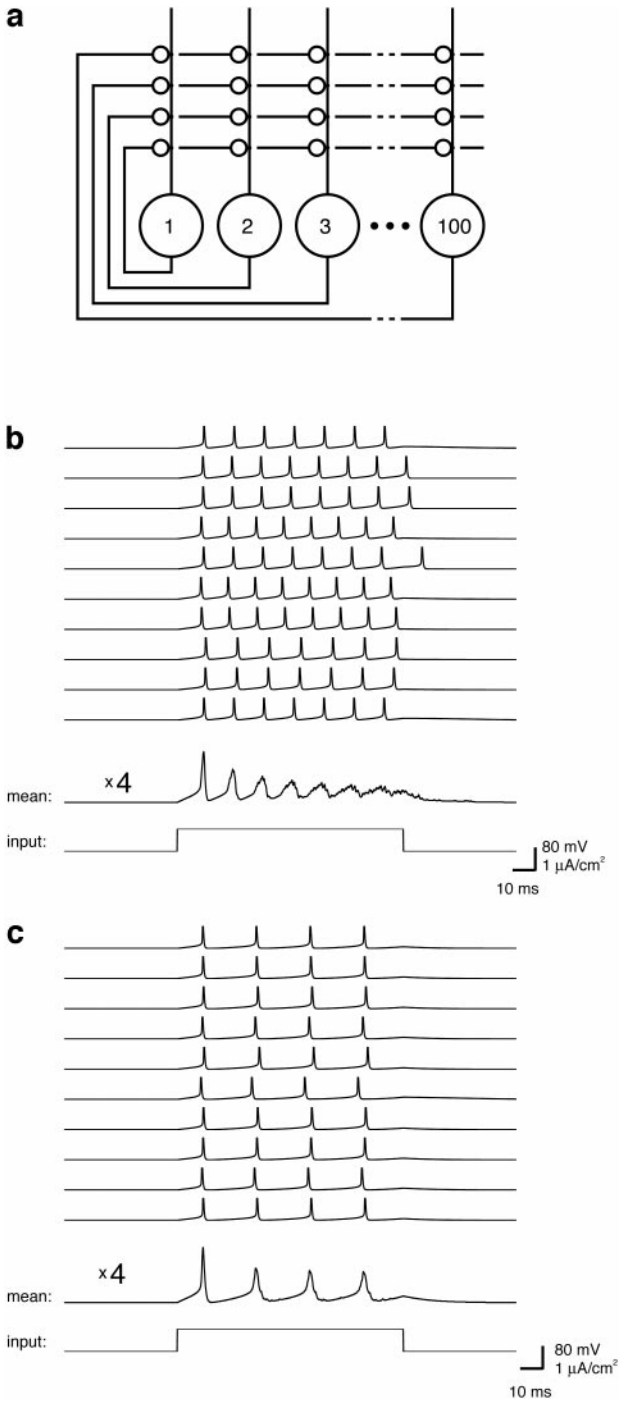

FIG. 9. Examples from simulations of the network model producing evoked gamma responses. (a) The network was constructed from 100 Hodgkin–Huxley model neurons with GABAergic connections. (b) Uncoupled network (g_{GABA_A} = 0 mS/cm^2). The first 10 traces are the membrane potentials selected randomly from 10 of the 100 neurons. The "mean" trace is the average of the 100 membrane potentials (multiplied by 4) and the "input" trace the average of the depolarizing input current to the cells. During the 100 ms of depolarization, the synchrony between the cells is lost. (c) All-to-all GABAergic connected cells (g_{GABA_A} = 0.1 mS/cm^2). The synchrony is maintained during the period of depolarization. The mean input current was $I_{app,\mu}$ = 1 μA/cm^2 and the standard deviation I_σ = 0.05 μA/cm^2.

ratory alkalosis. Several studies have demonstrated that alkalosis enhances neuronal excitability and alters synaptic transmission (e.g., Wyke, 1963; Jarolimek *et al.*, 1989; Chesler and Kaila, 1992; Lee *et al.*, 1996). However, it is far from clear how the effects of hypocapnia could modulate the neuronal substrates responsible for the generation of the evoked gamma responses. Extensive theoretical and experimental work on the rat hippocampus suggests that networks of interneurons coupled with GABAergic connections are responsible for rhythmogenesis and neuronal synchronization underlying gamma oscillations (Whittington *et al.*, 1995; Traub *et al.*, 1996; Wang and Buzsaki, 1996; Fisahn *et al.*, 1998; Penttonen *et al.*, 1998; Bracci *et al.*, 1999; Palva *et al.*, 2000).

To find out whether visually evoked gamma responses in the occipital cortex could be produced by a network of interneurons, we demonstrated by numerical simulations that a model network of interneurons can produce evoked gamma responses when depolarized with a short current pulse. Further simulations revealed that an increase in $GABA_A$ conductance can explain the increase in evoked gamma responses as a consequence of a tightening of neuronal synchrony (Fig. 10). An increase in synchrony in response to enhanced inhibition is well explained theoretically (Lytton and Sejnowski, 1991; Vreeswijk *et al.*, 1994; Gerstner *et al.*, 1996). When GABAergic transmission

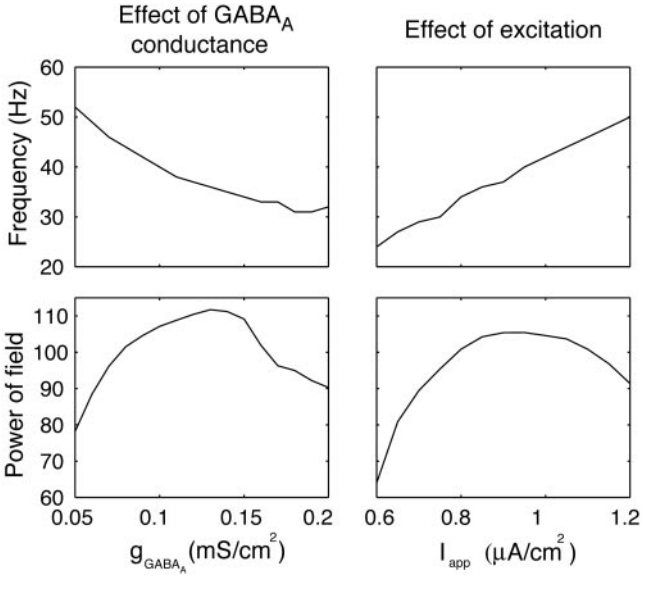

FIG. 10. The properties of the evoked gamma responses produced by the network model as a function of $GABA_A$ mediated conductance. The frequency of evoked gamma responses decreases as a function of inhibitory coupling g_{GABA}, whereas the synchronization measured by the power of the field in the gamma band increases and then decreases (left). The frequency of the evoked gamma responses increases as a function of input current, whereas the synchronization increases and then decreases (right).

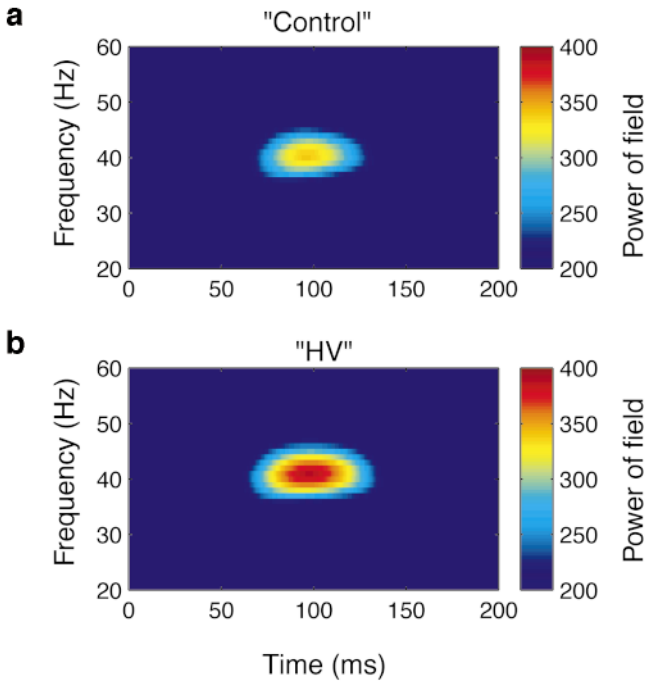

FIG. 11. Time-frequency representations of the power of the simulated gamma responses. (a) During the period of depolarization (50 to 150 ms), the gamma synchronization of the network is observed as an increase in power at 40 Hz for $g_{GABA_A} = 0.06$ mS/cm^2 and $I_{app,\mu} = 0.8$ μA/cm^2. (b) The gamma synchronization for $g_{GABA_A} = 0.1$ mS/cm^2 and $I_{app} = 1.0$ μA/cm^2, simulating the changes that take place during HV.

increased further, the gamma response eventually decreased, since the enhanced inhibition prevented some neurons from firing. The increased $GABA_A$ conductance always decreased the gamma frequency as it took longer for the membrane potentials to reach the firing threshold. A rise in intrinsic excitability did also lead to an increase in neuronal gamma synchrony which, however, was associated with increased frequency. We therefore propose that the strengthening of evoked gamma responses, without a change in frequency, is a consequence of an increase in both excitability and in $GABA_A$-mediated inhibition (Fig. 11). This hypothesis is in line with a recent study on rat hippocampal slices, where hypocapnia enhanced the temporal stability (measured using the decay of the autocorrelation of the field potential) of carbachol-induced gamma oscillations (Stenkamp *et al.*, 2001). Consistent with our model, the increase in temporal stability co-occurred with enhanced $GABA_A$ transmission.

Recently, the possible role of gap junctions on interneuronal synchronization has received a lot of attention (Galarreta and Hestrin, 1999; Gibson *et al.*, 1999; Tamas *et al.*, 2000; Traub and Bibbig, 2000). Since the conductivity of gap junctions increases with intracellular pH (Spray *et al.*, 1981), it is possible that respiratory alkalosis could affect the gap junctions and thus the properties of the interneuronal network. In the study by Stenkamp *et al.*, (2001), a rise in intracellular pH of hippocampal neurons decreased the temporal stability and slightly increased the frequency of the carbachol-induced gamma oscillations. Based on this finding, one might speculate that changes in the properties of gap junctions are not responsible for the increase in the gamma responses with HV. Nevertheless, further theoretical and experimental work is required to investigate how changes in gap junction conductivity affect the synchronization properties in various types of oscillatory networks.

In addition to changes in brain pH (Petroff *et al.*, 1985; Yaksh and Anderson, 1987; Andrews *et al.*, 1994), HV leads to reductions in cerebral blood flow and a consequent fall in oxygen tension (Severinghaus and Lassen, 1967). The possibility that the latter effect might have an influence on our present results cannot be excluded, but it should be noted here that the hypocapnia-induced stabilization of spontaneous gamma activity in the *in vitro* experiments (Stenkamp *et al.*, 2001) was observed at the fixed ambient level (95–99%) of pO_2.

Several studies suggest that evoked gamma activity plays a role in early sensory processing. Evoked EEG gamma responses are elicited by a number of different visual stimuli (Tallon-Baudry *et al.*, 1996; 1997) and are increased with selective attention (Herrmann and Mecklinger, 2001). Accordingly, single cell recordings in monkeys have demonstrated that neurons in the primary visual cortex fire in phase with gamma oscillations phase-locked to visual stimuli and that the synchronization in the gamma band was stronger in response to attended than unattended stimuli (Fries *et al.*, 2001).

The mechanisms by which a network of inhibitory interneurons can generate spontaneous gamma activity in the hippocampus have been explored in great detail. In this work we have demonstrated that related mechanisms could be responsible for generating evoked gamma responses in the human visual cortex. Future studies in which the properties of the interneuronal network are manipulated are required to further elucidate the physiological mechanisms generating the evoked gamma responses.

ACKNOWLEDGMENTS

This research was supported by the Danish Medical Research Council and the Academy of Finland. The MRIs were acquired at the Department of Radiology of the Helsinki University Central Hospital. We thank Matias Palva and Satu Palva for valuable comments on this manuscript.

REFERENCES

Andrews, R. J., Bringas, J. R., and Alonzo, G. 1994. Cerebrospinal fluid pH and PCO2 rapidly follow arterial blood pH and PCO_2 with changes in ventilation. *Neurosurgery* **34:** 466–470.

Bostem, F. 1976. Hyperventilation. In *Handbook of Electroencephalography and Clinical Neurophysiology* (A. Remond, Ed.), pp. 74–88. Elsevier, Amsterdam.

Bracci, E., Vreugdenhil, M., Hack, S. P., and Jefferys, J. G. 1999. On the synchronizing mechanisms of tetanically induced hippocampal oscillations. *J. Neurosci.* **19:** 8104–8113.

Chesler, M., and Kaila, K. 1992. Modulation of pH by neuronal activity. *Trends Neurosci.* **15:** 396–402.

Davies, H. D., Carroll, W. M., and Mastaglia, F. L. 1986. Effects of hyperventilation on pattern-reversal visual evoked potentials in patients with demyelination. *J. Neurol. Neurosurg. Psychiatry* **49:** 1392–1396.

Diest, I. V., Stegen, K., de Woestijne, K. P. V., Schippers, N., and den Bergh, O. V. 2000. Hyperventilation and attention: Effects of hypocapnia on performance in a stroop task. *Biol. Psychol.* **53:** 233–252.

Fisahn, A., Pike, F. G., Buhl, E. H., and Paulsen, O. 1998. Cholinergic induction of network oscillations at 40 Hz in the hippocampus *in vitro. Nature* **394:** 186–189.

Fries, P., Reynolds, J. H., Rorie, A. E., and Desimone, R. 2001. Modulation of oscillatory neuronal synchronization by selective visual attention. *Science* **291:** 1560–1563.

Galarreta, M., and Hestrin, S. 1999. A network of fast-spiking cells in the neocortex connected by electrical synapses. *Nature* **402:** 72–75.

Gavriysky, V. S. 1991. Influence of a twofold voluntary hyperventilation on visually evoked cortical potentials and human pupillogram. *Doc. Ophthalmol.* **77:** 213–224.

Gerstner, W., van Hemmen, J. L., and Cowan, J. D. 1996. What matters in neuronal locking? *Neural. Comput.* **8:** 1653–1676.

Gibson, J. R., Beierlein, M., and Connors, B. W. 1999. Two networks of electrically coupled inhibitory neurons in neocortex. *Nature* **402:** 75–79.

Hämäläinen, M., Hari, R., Ilmoniemi, R. J., Knuutila, J., and Lounasmaa, O. V. 1993. Magnetoencephalography—Theory, instrumentation, and applications to noninvasive studies of the working human brain. *Rev. Mod. Phys.* **65:** 413–497.

Hasnain, M. K., Fox, P. T., and Woldorff, M. G. 1998. Intersubject variability of functional areas in the human visual cortex. *Hum. Brain Mapp.* **6:** 301–315.

Herrmann, C. S., and Mecklinger, A. 2001. Gamma activity in human EEG is related to high-speed memory comparisons during object selective attention. *Vis. Cogn.* **8:** 593–608.

Hodgkin, A., and Huxley, A. 1952. A quantitative description of membrane current and its application to conduction and excitation in nerve. *J. Physiol. (London)* **117:** 500–544.

Huttunen, J., Tolvanen, H., Heinonen, E., Voipio, J., Wikstrom, H., Ilmoniemi, R. J., Hari, R., and Kaila, K. 1999. Effects of voluntary hyperventilation on cortical sensory responses. Electroencephalographic and magnetoencephalographic studies. *Exp. Brain Res.* **125:** 248–254.

Jarolimek, W., Misgeld, U., and Lux, H. D. 1989. Activity dependent alkaline and acid transients in guinea pig hippocampal slices. *Brain Res.* **505:** 225–232.

Koch, C., and Segev, I. 1998. *Methods in Neuronal Modeling.* The MIT Press, Cambridge, MA,

Kronland-Martinet, R., Morlet, J., and Grossmann, A. 1987. Analysis of sound patterns through wavelet transforms. *Int. J. Patt. Recogn. Art. Intell.* **1:** 273–302.

Lee, J., Taira, T., Pihlaja, P., Ransom, B. R., and Kaila, K. 1996. Effects of CO_2 on excitatory transmission apparently caused by changes in intracellular pH in the rat hippocampal slice. *Brain Res.* **706:** 210–216.

Lytton, W. W., and Sejnowski, T. J. 1991. Simulations of cortical pyramidal neurons synchronized by inhibitory interneurons. *J. Neurophysiol.* **66:** 1059–1079.

McBain, C. J., and Fisahn, A. 2001. Interneurons unbound. *Nat. Rev. Neurosci.* **2:** 11–23.

Niedermeyer, E., and Lopez da Silva, F. 1993. *Electroencephalography. Basic Principles, Clinical Applications, and Related Fields.* 3rd ed. Williams and Wilkins.

Palva, J. M., Lamsa, K., Lauri, S. E., Rauvala, H., Kaila, K., and Taira, T. 2000. Fast network oscillations in the newborn rat hippocampus *in vitro. J. Neurosci.* **20:** 1170–1178.

Parkkonen, L. T., Simola, J. T., Tuoriniemi, J. T., and Ahonen, A. I. 1999. An interference suppression system for multichannel magnetic field detector arrays. *In Recent Advances in Biomagnetism* (T. Yoshimoto, M. Kotani, S. Kuriki, H. Karibe, and N. Nakasato, Eds.), pp. 13–16. Tohoku Univ. Press, Sendai, Japan.

Penttonen, M., Kamondi, A., Acsady, L., and Buzsaki, G. 1998. Gamma frequency oscillation in the hippocampus of the rat: intracellular analysis *in vivo. Eur. J. Neurosci.* **10:** 718–728.

Petroff, O. A., Prichard, J. W., Behar, K. L., Rothman, D. L., Alger, J. R., and Shulman, R. G. 1985. Cerebral metabolism in hyper- and hypocarbia: 31 P and 1 H nuclear magnetic resonance studies. *Neurology* **35:** 1681–1688.

Portin, K., Vanni, S., Virsu, V., and Hari, R. 1999. Stronger occipital cortical activation to lower than upper visual field stimuli. Neuromagnetic recordings. *Exp. Brain Res.* **124:** 287–294.

Press, W. H., Teukolsky, S. A., Vetterling, W. T., and Flannery, B. P. 1997. *Numerical Recipes in C.* Cambridge Univ. Press, USA.

Severinghaus, J. W., and Lassen, N. 1967. Step hypocapnia to separate arterial from tissue PCO_2 in the regulation of cerebral blood flow. *Circ. Res.* **20:** 272–278.

Sinkkonen, J., Tiitinen, H., and Näätänen, R. 1995. Gabor filters: an informative way for analysing event-related brain activity. *J. Neurosci. Methods* **56:** 99–104.

Somjen, G. G., and Tombaugh, G. C. 1998. pH modulation of neuronal excitability and central nervous system functions. In *pH and Brain Function* (K. Kaila and B. R. Ransom, Eds.), pp. 373–393. Wiley-Liss.

Spray, D. C., Harris, A. L., and Bennett, M. V. 1981. Gap junctional conductance is a simple and sensitive function of intracellular pH. *Science* **211:** 712–715.

Stenkamp, K., Palva, M., Uusisaari, M., Schuchmann, S., Schmitz, D., Heinemann, U., and Kaila, K. 2001. Enhanced temporal stability of cholinergic hippocampal gamma oscillations following respiratory alkalosis in vitro. *J. Neurophys.* **85:** 2063–2069.

Talairach, J., and Tournoux, O. 1988. *Co-planar Stereotaric Atlas of the Human Brain.* Thieme, New York.

Tallon-Baudry, C., and Bertrand, O. 1999. Oscillatory gamma activity in humans and its role in object representation. *Trends Cogn. Sci.* **3:** 151–162.

Tallon-Baudry, C., Bertrand, O., Delpuech, C., and Permier, J. 1997. Oscillatory gamma-band (30–70 Hz) activity induced by a visual search task in humans. *J. Neurosci.* **17:** 722–734.

Tallon-Baudry, C., Bertrand, O., Delpuech, C., and Pernier, J. 1996. Stimulus specificity of phase-locked and non-phase-locked 40 Hz visual responses in human. *J. Neurosci.* **16:** 4240–4249.

Tamas, G., Buhl, E. H., Lorincz, A., and Somogyi, P. 2000. Proximally targeted GABAergic synapses and gap junctions synchronize cortical interneurons. *Nat. Neurosci.* **3:** 366–371.

Traub, R. D., and Bibbig, A. 2000. A model of high-frequency ripples in the hippocampus based on synaptic coupling plus axon–axon gap junctions between pyramidal neurons. *J. Neurosci.* **20:** 2086–2093.

Traub, R. D., Jefferys, J. G. R., and Whittington, M. A. 1999. *Fast Oscillations in Cortical Circuits.* MIT Press.

Traub, R. D., Whittington, M. A., Colling, S. B., Buzsaki, G., and Jefferys, J. G. 1996. Analysis of gamma rhythms in the rat hippocampus *in vitro* and *in vivo. J. Physiol. (London)* **493:** 471–484.

Vreeswijk, C. V., Abbott, L. F., and Ermentrout, G. B. 1994. When inhibition not excitation synchronizes neural firing. *J. Comput. Neurosci.* **1:** 313–321.

Wang, X. J., and Buzsaki, G. 1996. Gamma oscillation by synaptic inhibition in a hippocampal interneuronal network model. *J. Neurosci.* **16:** 6402–6413.

Whittington, M. A., Traub, R. D., and Jefferys, J. G. 1995. Synchronized oscillations in interneuron networks driven by metabotropic glutamate receptor activation. *Nature* **373:** 612–615.

Wyke, B. 1963. *Brain Function and Metabolic Disorders. The Neurological Effects of Changes in Hydrogen Ion Concentration*. Butterworths, London.

Yaksh, T. L., and Anderson, R. E. 1987. *In vivo* studies on intracellular pH, focal flow, and vessel diameter in the cat cerebral cortex: Effects of altered CO2 and electrical stimulation. *J. Cereb. Blood. Flow. Metab.* **7:** 332–341.